Laboratory Noble Gas Migration Experiments Through Rock

S31A-2693

Scott Broome[1], Avery Cashion[1], Joshua Feldman[1], Aviva J Sussman[2], Erika Swanson[2], Jennifer Wilson[2], Jason Heath[1], Kristopher Kuhlman[1]

Corresponding Author: Scott Broome, stbroom@sandia.gov

[1]Sandia National Laboratories, Albuquerque, New Mexico

[2]Los Alamos National Laboratory, Los Alamos, New Mexico

Exceptional service in the national interest

Introduction and Background

Introduction

The Underground Nuclear Explosion Signature Experiment (UNESE) is a multi-laboratory effort to improve U.S. capabilities to detect, locate, identify, and characterize underground nuclear explosions. Here we present a lab-scale experiment developed to test advective gas transport though rock samples at in-situ conditions, and results of tests performed at ambient conditions on rocks collected from the site of a field-scale experiment. Gas transport results are compared to pore and fracture networks of the same samples characterized by micro-CT and petrographic microscopy. Future work will use this experimental apparatus to interrogate advective gas transport at a variety of relevant pressure and temperature conditions.

Background

Ionizing radiation produced by a nuclear explosion result in the production of radioactive isotopes of argon, xenon, and other gases which have extremely low atmospheric concentrations. ^{37}Ar (half-life: 34.05 days) and ^{133}Xe (half-life: 5.25 days) are useful tracers of UNEs because they have low detection thresholds and their short half-lives can be used to determine when the UNE took place. UNEs conducted at the NNSS (formerly NTS) in the early 1990s showed that more diffusive gases reached the surface more slowly than less diffusive gases. This non-intuitive observation was explained by Carrigan et al. (1996) as the result of more diffusive ^{37}Ar diffusing into pores more readily than SF_6 (a proxy for ^{133}Xe), and therefore being delayed relative to SF_6 during barometric pumping. Carrigan et al., (1996) suggested that naturally occurring fracture networks and faults were the primary conduits for these radiogenic gases and, for this reason, proposed that collection of gas samples for UNE detection should prioritize faults and fracture networks over proximity to ground zero. To examine the effect of different rock types on flow and transport properties of Ar, Xe, and SF_6, we have developed an apparatus and methodology capable of simulating conditions of an UNE. For these laboratory experiments, samples were run at surface pressure and temperature conditions, and barometric pumping was not implemented, however future experiments will simulate these parameters. Additionally, in order to understand which fractures were responsible for the migration of gases, the rocks and fractures in which the laboratory experiments took place were well characterized by a suite of techniques including micro-CT and optical microscopy. Representative samples were selected from core recovered from a borehole adjacent to a legacy UNE. The five lithologies included in this study are: Rhyolitic lava (RL), zeolitic nonwelded tuff (ZN), partially welded tuff (PW), vitric nonwelded tuff (VN), and strongly welded tuff (SW). Microfracture densities and fracture properties such as sealing are reported to identify which fractures served as gas migration pathways. As part of this ongoing project, we are currently mapping the fractures in three-dimensions.

Experimental Apparatus and Methodology

Experimental Design

In addition to diffusivity, it is likely that dissolution of gas into water plays a role in the retardation of gas transport rates, and therefore any experimental apparatus should include the ability to adjust the water saturation of a sample. While this experiment used dry samples, future testing should include partial water saturation. Four gases were selected for the gas mix to interrogate the transport properties of different samples: N_2 (80%), Ar (6.67%), Xe (6.67%), and SF_6 (6.67%). In terms of the extraction line, samples were prepared from 2.5" core by end-grinding and jacketing in UV-Cure epoxy with a porous metal frit and end caps on each end. Samples are connected to the extraction line and can be pumped to 0.100 mbar or better. Relative to the sample, the upstream volume consists of a gas reservoir we call 'the bolus' which has a known volume of 50.2 mL and a pressure gauge with a range from 500 – 2000 mbar. A manual valve separates the upstream volume from the sample. Downstream of the sample are two pressure gauges (a Pirani gauge and a Cold-Cathode/Pirani combo gauge), and the inlet leak valve. The leak valve is capable of high-precision reproducibility and allows the pressure in the extraction line to go from 0.050 mbar to 2000 mbar without raising the vacuum in the quadrupole mass analyzer above 1x10^{-5} mbar. The leak valve is set prior to running any experiments, and is not changed throughout the experiment.

Procedures

For each sample, three sets of runs are conducted at different initial pressures of the gas in the boblus: low pressure (~200 mbar), medium pressure (~1500 mbar), and high pressure (~2000 mbar).

1. Prepare and jacket sample
2. Install sample in line
3. Vacuum line to 0.100 mbar or below
4. Charge bolus with gas mixture up to 200, 1500, and 2000 mbar (nominally)
5. Vacuum line to 0.100 mbar or below
6. Configure valves for analysis and begin recording on quadrupole
7. Allow baselines to come to an equilibrium state
8. Open bolus
9. Record until upstream and downstream pressures equalize
10. Measure the ion current of the different gas species with QMA in real time

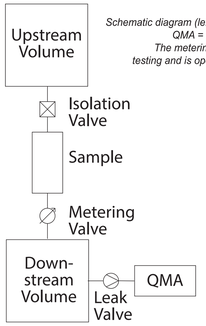

Schematic diagram (left) and photo (below) of the extraction line. QMA = quadrupole mass analyzer. The metering valve is only used for system testing and is opened all the way during sample runs.

Photo of the Rhyolitic Lava jacketed and ready to be installed in the extraction line.

A close-up photo of the leak valve. The knurled knobs on top are for adjusting the leak rate.

Experimental Results

Experiments are conducted until the upstream pressure and downstream pressure equalize, the timing of which is different from sample to sample. Upon opening the bolus to the system, pressure downstream begins to increase immediately and is proportional to the decrease in the pressure upstream. The concentration of Ar, Xe, and SF_6 in the QMS begins to increase quickly, but not immediately, and the delay time is longer in less permeable samples. At the field scale, SF_6 was observed before Xe, which was observed before Ar, but in the lab we see Ar break through first, followed by Xe and SF_6 which are close together and change positions from run to run. The Ar and Xe data are corrected for atmospheric composition, and the SF6 data are summed. All data are normalized to the standardized gas mixture (which is composed of 6.67% of each Ar, Xe, and SF_6, and 80% N_2). The leak valve, being essentially a choked orifice, will fractionate the gases. The leak valve was set prior to experimentation such that pressure in the quadrupole did not rise above 1x10^{-5} mbar with the upstream side exposed to atmosphere. Tests were done to assess the amount of fractionation the leak valve introduced, but the amount was insignificant relative to the uncertainty in our measurements.

One assumption we made when designing the extraction line was that the volume of gas sampled through the leak valve into the QMS was very small compared to the downstream volume. For the 200 mbar runs, the absolute amount of gas in the downstream volume is small enough that this assumption is partially violated, which is why the gas concentrations never reach .0667 and the trends fall off after reaching their maximum. Because of how the leak valve was set (see above) this cannot be avoided in our current setup, however the model appears to be insensitive to this factor.

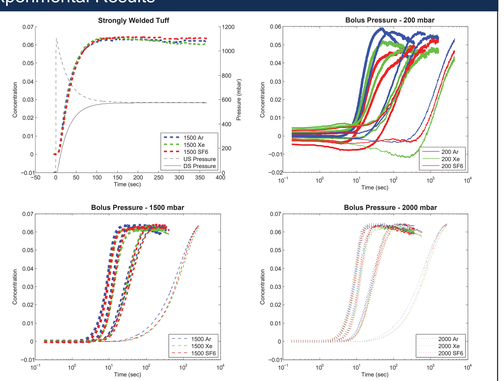

Plot for individual test (upper left). Gas concentration vs time plots (right and lower left). Line thickness represents both rock type (VN, PW, SW, ZN, RL--see above) and corresponding permeability.

Sample Characterization

Rhyolitic Lava

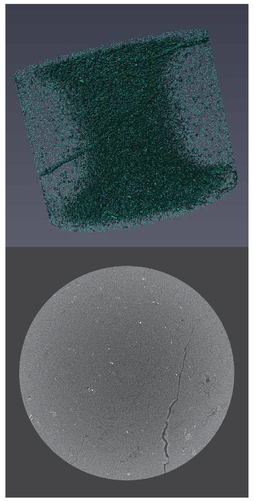

Micro-CT

After gas flow testing, the endcaps and metal frits were removed from the samples. The samples were scanned on a Micro-CT and the data processed in PerGeos.

Petrography

The samples were impregnated with epoxy, and sliced; the slices were made into thin sections for petrographic characterization and analysis. All thin section images and microfracture data were collected using an Olympus Polarizing Microscope equipped with a digital camera and CellSens imaging software. Figures show CT data and photomicrographs of the Rhyolitic Lava and Vitric Nonwelded Tuff, which were selected to illustrated the least and most permeable samples we tested, respectively. The left column are all images of the Rhyolitic Lava, and the right column are all images of the Vitric Nonwelded Tuff.

Vitric Nonwelded Tuff

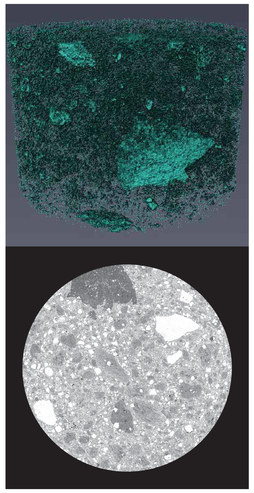

Images from Micro-CT scans of the Rhyolitic Lava and Vitric Nonwelded Tuff. The core is approximately 2.5 inches in diameter and 2.0 inches tall.The top row shows 3D models of open space in the two samples created from CT scans of the core. The lower row shows slices of the cores at representative depths in the core. The hour-glass shadow structure in the Rhyolitic lava is interpreted as an artifact of the scan, however the linear features visible are fractures, which are also visible in the slice. The Vitric Nonwelded Tuff is heterogeneous and fractures are below the resolution of the CT scan (approximately 13 um).

Zeolitic Nonwelded Tuff

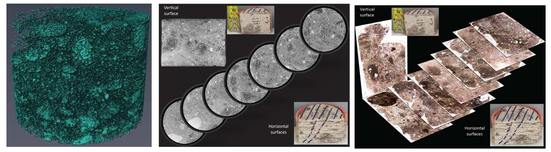

Micro-CT 3D model (left), Micro-CT (middle) and photomicrograph (right) slices of zeolitic nonwelded tuff. Micro-CT slices are rotated relative to photomicrograph slices, but are from approximately the same part of the sample. Large-scale fractures visible in the CT and photomicrograph slices are not visible in the 3D model, suggesting they are just below the resolution of the CT modeling capabilities or they are obscured by the pores.

Rhyolitic Lava

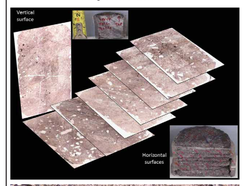

Vitric Nonwelded Tuff

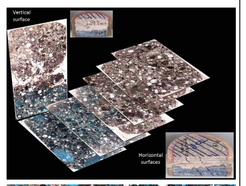

Stack of Rhyolitic Lava slices (left) for context. Each slice is approximately 1.5 inches in length and 0.8 inches in width and are taken at 0.25-inch intervals from the core. Stack of Vitric Nonwelded Tuff slices (right) for context. Each slice is approximately 1.5 inches in length and 0.8 inches in width and are taken at 0.25 inch intervals from the core. Blue-dyed epoxy was introduced to the bottom portion of the sample in order to increase sample integrity during slicing.

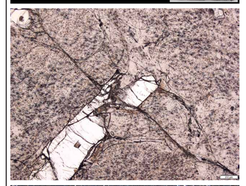

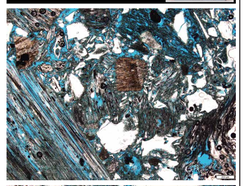

Photomicrograph (left) of sealed microfracture transecting rhyolitic glass and phenocryst. Field of view is 2.6 mm; image taken under plane light and is oriented within a vertical slice of the core. Photomicrograph (right) showing the variety of pore spaces (blue) and heterogeneity of grains in Vitric Nonwelded Tuff, including vesicular pumice, phenocrysts, lithic fragments, glass shards, and micron-sized ash. Field of view is 2.6 mm; image taken under plane light and is oriented within a vertical slice of the core.

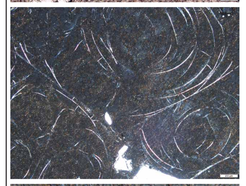

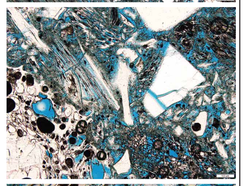

Photomicrograph (left) of multiple perlitic microfractures sealed with a highly birefringent mineral. Most microfractures in this rock type resemble the ones in this image, which are sealed and converge on each other rather than transecting large portions of the rock. Field of view is 2.6 mm; image taken under plane polarized light and is oriented within a horizontal slice of the core. Photomicrograph (right) of open microfractures that transect pumice and phenocrysts, thereby connecting previously isolated pore spaces. Field of view is 1.3 mm; image taken under plane light and is oriented within a horizontal slice of the core.

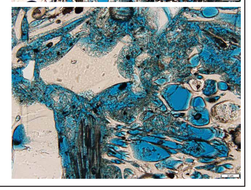

Photomicrograph (left) of prominently sealed microfractures, as well as less visible, very low-aperture (<3 um) open microfractures, cutting through rhyolitic glass. Field of view is 0.65 mm; image taken under plane polarized light and is oriented within a horizontal slice of the core. Photomicrograph (right) showing the variety of pore morphology and connectivity in Vitric Nonwelded Tuff. Pore morphology ranges from isolated pores within pumice to highly interconnected pathways with varying amounts of micron-sized ash. Field of view is 0.65 mm; image taken under plane light and is oriented within a horizontal slice of the core.

Modeling

Approach

The flow of the N2, Ar, Xe, and SF6 mixture is modeled using PFLOTRAN with the Klinkenberg expression for effective gas permeability:

$$k_g = k_l\left(1+\frac{b}{\bar{p}}\right)$$

where kl is the absolute (or liquid) permeability, b is the Klinkenberg coefficient, and p is the average pressure. In PFLOTRAN, the Klinkenberg coefficient is broken into two components

$$b = Bk_l^{\,A}$$

The parameter estimation code PEST (Doherty, 2015) is used to obtain kl, b, and the porosity φ.

One set of parameters are estimated from a suite of three gas-flow tests. The same sample is used in all three tests (approximately 200, 1500, and 2000 mbar initial pressure in bolus), and PEST is used to estimate a parameter set that best fits all three tests simultaneously.

Model domain and boundary conditions

The flow system is discretized and treated as a one-dimensional flow path. The upstream pressure boundary condition is applied to match the measured pressure. The downstream boundary condition represented the pressure within the QMS.

Flow modeling results

1. The one-dimensional single-phase gas flow model reproduces the total pressure observed in the experiments quite well. The model captures both the magnitude and characteristic shape of the observed pressure responses.
2. Klinkenberg coefficients are necessary for capturing the flow behavior for all tests except the highest absolute permeability sample.
3. The lowest pressure tests (approximately 200 mbar) are most sensitive to the Klinkenberg coefficient, and lower permeability samples are more sensitive to this parameter than higher permeability samples.
4. The higher-pressure tests are more sensitive to the absolute permeability and porosity of the sample than the lower-pressure tests, but all three tests in each set contribute to the estimate of these parameters.
5. The downstream permeability of the leak valve to the quadrupole mass spectrometer is the least sensitive parameter in all tests at all pressures.

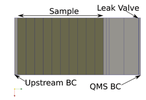

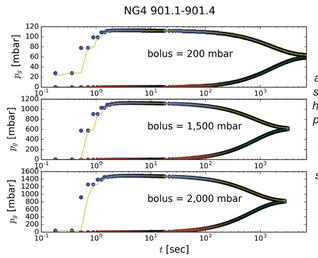

Observed upstream (blue dots) and downstream (red dots) pressures for lowest (top left; RL) and highest (bottom left; VN) absolute permeability samples. Model predictions downstream given by green line. Upstream observed pressure was assigned at upstream Dirichlet boundary condition.

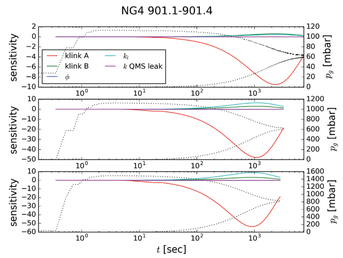

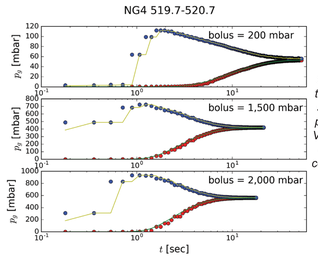

Sensitivity of model parameters through time for least permeable sample (top right; RL) and most permeable sample (bottom right; VN). Observed pressure given by dotted line. Colored curves are columns of Jacobian matrix at optimum.

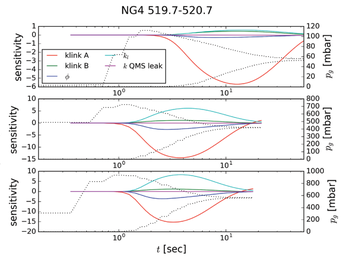

Summary and Conclusions

Sample ID	porosity, φ (model)	absolute (liquid) permeability, k_l (m^2) (model)	Klinkenberg coefficient, b (Pa) (model)	porosity, φ (measured adjacent to sample with helium porosimeter)	apparent permeability, k_{app} (m^2) (measured on sample)	open microfracture density (mf/mm) measured in horizontal plane (averaged from 8 thin sections)	open microfracture density (mf/mm) measured in vertical plane
NG4 901.1-901.4 (RL)	0.01	1.18E-16	3.87E+04	0.03	9.0E-17	1.3	1.4
NG4 1127.8-1128.1 (ZN)	0.11	4.24E-15	2.71E+03	0.17	1.2E-15	0.5	0.2
NG4 67.0-67.8 (SW)	0.09	4.85E-15	9.61E+03	0.12	2.3E-15	0.5	0.5
NG4 29.6-30.2 (PW)	0.26	2.83E-14	1.34E+04	0.29	1.9E-14	0.2	0.1
NG4 519.7-520.7 (VN)	0.34	8.81E-14	7.16E+03	0.23	5.7E-14	0.8	0.6

- We have developed and tested an experimental apparatus to measure flow and transport characteristics of radioisotopic noble gases at in-situ pressure and temperature.
- The apparatus includes advective flow and transport, with a interpretative modeling techniques that obtains the non-Darcy gas flow parameter (Klinkenberg coefficient).
- The above table shows reasonable good agreement between the standard measurements, flow modeling, and optically determined porosity and permeability.
- The rock permeability shows an inverse relationship with micro-fracture density.

Future work

- investigate the contribution of the matrix-vs-fracture on the permeability
- flow testing and modeling under triaxial stress states to investigate stress sensitivity for the given porosity and fracture microstructure.
- variable water content to investigate effects on breakthrough of gases
- collection of macrofracture density data
- determination of macro- and micro- fracture apertures and orientations

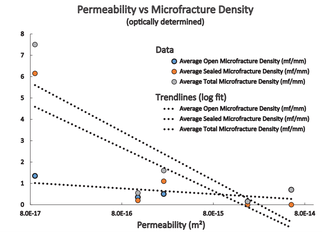

References and Acknowledgements

References

Carrigan, C. R., Heinle, R. A., Hudson, G. B., Nitao, J. J., and Zucca, J. J., Trace gas emissions on geological faults as indicators of underground nuclear testing. Nature. Vol. 382. 8/8/1996.

Doherty, J., 2015. Calibration and Uncertainty Analysis for Complex Environmental Models. Watermark Numerical Computing, Brisbane, Australia. ISBN: 978-0-9943786-0-6.

Acknowledgements

Sandia National Laboratories is a multi-mission laboratory managed and operated by Sandia Corporation, a wholly owned subsidiary of Lockheed Martin Corporation, for the U.S. Department of Energy's National Nuclear Security Administration under contract DE-AC04-94AL85000.